

JHK Spectra of the $z = 2.39$ Radio Galaxy 53W002 ¹

Kentaro MOTOHARA^{2,3}Toru YAMADA^{4,6}, Fumihide IWAMURO³, Ryuji HATA³, Tomoyuki TAGUCHI³, Takashi HARASHIMA³,
Toshinori MAIHARA^{3,5}, Masanori IYE⁴, Chris SIMPSON², and Michitoshi YOSHIDA^{4,7}² *Subaru Telescope, National Astronomical Observatory of Japan,
650 North A'ohoku Place, Hilo, HI 96720, USA**motohara@naoj.org*³ *Department of Physics, Kyoto University, Kitashirakawa, Kyoto 606-8502*⁴ *Optical and Infrared Astronomy Division, National Astronomical Observatory of Japan, Mitaka, Tokyo 181-8588*⁵ *Department of Astronomy, Kyoto University, Kitashirakawa, Kyoto 606-8502*⁶ *Astronomical Institute, Tohoku University, Aoba-ku, Sendai, Miyagi 980-8578*⁷ *Okayama Astrophysical Observatory, National Astronomical Observatory of Japan,
Kamogata-cho, Asakuchi-gun, Okayama 719-0232*

(Received 2000 December 19; accepted 2001 March 18)

Abstract

We present low-resolution, near-IR *JHK* spectra of the weak $z = 2.39$ radio galaxy 53W002, obtained with the OH-airglow Suppressor spectrograph (OHS) and Cooled Infrared Spectrograph and Camera for OHS (CISCO) on the Subaru Telescope. They cover rest-frame wavelengths of 3400–7200 Å, and the emission lines of [O II] λ 3727, H β , [O III] λ 4959, 5007, H α , [N II] λ 6548, 6583 and [S II] λ 6716, 6731 were detected. Using the H α /H β line ratio, we find an extinction of $E(B - V) = 0.14$. The emission-line ratios are reproduced by a cloud of electron density $n_e = 1 \times 10^{3-4}$ (cm⁻³) with solar metallicity, ionized by an $\alpha = -0.7$ power-law continuum with ionizing parameter $U = 1 \times 10^{-3}$. In addition to these emission lines, we make the first spectroscopic confirmation of the Balmer discontinuity in a high- z radio galaxy. Together with rest-frame UV photometry from the literature, we show that at least 1/3 of the present stellar mass was formed in the current starburst. The stellar mass was estimated to be $(1 - 1.4) \times 10^{11} M_\odot$ by one-component model fitting, which is smaller than that of typical $z \sim 1$ B2/6C radio galaxies. We suggest that 53W002 is currently assembling a large part of its stellar mass through merger events with the surrounding sub-galactic clumps, some of which can be identified with the L α emitters detected in narrow-band imaging. After a few such events over the next few Gyr, 53W002 will evolve into a massive elliptical galaxy.

Key words: galaxies: active — galaxies: individual (53W002) — galaxies: spectroscopy

1. Introduction

Many high- z field galaxies were discovered in the 1990s using the UV drop-out technique. However, these objects are rather faint, and infrared spectroscopy is difficult (Pettini et al. 1998). On the other hand, high- z radio galaxies are relatively bright, and their properties have been fairly well-studied. In addition, as the progenitors of present-day massive galaxies, they are important for studying galaxy formation.

53W002 is a $z = 2.39$ galaxy with relatively weak radio power ($S_{1.4\text{GHz}} \sim 50$ mJy; Windhorst et al. 1991), indicating that its AGN activity is not extreme and it

could therefore be suitable for a study of the underlying stellar population. Broad-band photometry (Windhorst et al. 1991) reveals a possible break at $\lambda_{\text{rest}} \sim 4000$ Å, and suggests recent star-formation activity from spectral model fitting. Its rest-frame UV spectrum suggests that the main-sequence turnoff age of the current starburst is 0.25–0.3 Myr (Windhorst et al. 1991). Radio observations have detected lines from CO molecules concentrated at the center of the galaxy (Yamada et al. 1995, Scoville et al. 1997, Alloin et al. 2000), which may be other indications of star-formation activity.

The radial surface brightness profile of 53W002, as revealed by HST, is well-modeled by a de Vaucouleurs profile, suggesting that the galaxy is already dynamically relaxed. A $V - I$ radial color gradient suggests that the

¹ Based on data collected at Subaru Telescope, which is operated by the National Astronomical Observatory of Japan.

center of the galaxy consists of a young population (0.3–0.5 Gyr), while older stars (0.5–1.0 Gyr) exist in the outer ($r > 10$ kpc) region (Windhorst et al. 1994).

Previous infrared spectroscopy has revealed the presence of the $H\alpha + [\text{N II}]$ lines in the K -band (Eales, Rawlings 1993), but a detailed discussion was precluded by their limited sensitivity. We have therefore carried out low-resolution infrared spectroscopy of 53W002 to investigate the properties of its emission-line clouds and underlying stellar population. For JH -band spectroscopy, we used a newly-commissioned instrument of the Subaru telescope, an OH-airglow suppression Spectrograph (OHS; Maihara et al. 1994, Iwamuro et al. 2001). OHS is a spectroscopic filter which eliminates almost all of the OH airglow lines in the JH -band, which are the major source of atmospheric background radiation at near-infrared wavelengths below $2 \mu\text{m}$. Using OHS, the background level is suppressed by 96% and the sensitivity becomes 1 magnitude fainter. The output from OHS is an undispersed beam from which OH airglow is suppressed; this is then sent to the Cooled Infrared Camera and Spectrograph for OHS (CISCO; Motohara et al. 1998) to acquire either images or spectra. CISCO can also be used as an ordinary infrared camera and spectrograph attached on either the Cassegrain or the Nasmyth focus of the telescope. For K -band spectroscopy, we used this mode.

We describe the observations and data reduction in section 2 and present the results in section 3. Discussions are given out in section 4 and we summarize our results in section 5. We adopt $H_0 = 65 \text{ km s}^{-1}$ and $q_0 = 0.1$ throughout this paper. The scale at $z = 2.39$ is thus $8.5 \text{ kpc arcsec}^{-1}$.

2. Observations and Data Reductions

2.1. K -Band Spectroscopy

K -band spectroscopy of 53W002 was carried out on 1999 May 10, with CISCO mounted at the Cassegrain focus of the Subaru telescope. The pixel scale was $0''.116/\text{pixel}$. A slit width of $0''.7$ provided a wavelength resolution of ~ 430 at $2.2 \mu\text{m}$. The position angle of the slit was set to 145° to include object 13 of Pascarelle et al. (1998) in the slit. Individual exposures were 200 s, and the telescope was nodded slightly ($\sim 5''$) after every six frames to provide sky subtraction. A total of 18 frames were taken for a total exposure time of 3600 s. The seeing size was $0''.4$. After the observation, the F0 star SAO 30082 was observed for correction of the atmospheric absorption.

2.2. H -Band Imaging and the JH -Band Spectroscopy

H -band imaging was carried out on 2000 May 20 and JH -band spectroscopy on 2000 May 20 and 23, with OHS

and CISCO mounted at the Nasmyth focus of the Subaru telescope. The pixel scale was $0''.105/\text{pixel}$.

The H -band images were taken with OHS in the imaging mode (see Iwamuro et al. 2001). The single exposure time was 50 s and the telescope was nodded every 3 frames by $10''$ in the east–west direction. A total of 12 frames were acquired, for an exposure time of 600 s.

The JH -band spectra were acquired using a $0''.95$ slit, providing a resolution of ~ 210 at $1.65 \mu\text{m}$. A position angle of 90° was used, which was aligned with the major axes of the radio and $L\alpha$ emission. After each 1000 s exposure, the telescope was nodded by $10''$ along the slit. We took 4 frames each day, and the total exposure time was 8000 s. The seeing size was $0''.6$. The F8 star SAO 30361 and F5 star SAO 30245 were observed after the target on May 20 and 23, respectively, for correcting the atmospheric absorption.

2.3. Data Reduction

The H -band frames were reduced through standard procedures of flat-fielding, sky subtraction, correction of bad pixels, residual sky subtraction, before registration and coaddition. Photometry was performed in a $1''.0 \times 2''.1$ aperture at a position angle of 90° , which is equal to the spectroscopic extraction aperture position. The flux in the H -band was $11.9 \pm 0.7 \mu\text{Jy}$, calibrated from an observation of FS 23.

The spectroscopic data were reduced in the standard manner of flat-fielding, sky subtraction, correction of bad pixels and residual sky subtraction. The spectra of the SAO F stars were used to correct for atmospheric extinction.

The wavelength scale of the K -band spectrum was calibrated from airglow lines in the raw frames. Such a procedure was impossible for the JH spectrum, since all the strong OH-lines were suppressed by OHS. We therefore calibrated our spectrum from another observation of CISCO without OHS, where OH lines were available. We checked the stability of the wavelength scale from all of the previous CISCO observations, and found the systematic error to be less than 0.5 pixels ($< 5 \text{ \AA}$).

Because the seeing size was less than the slit width for both spectroscopic observations, we assumed the error in the wavelength calibration to be $1/4$ of the slit width, i.e., $\sim \pm 13 \text{ \AA}$ (1.5 pixels) for the K -band and $\sim \pm 22 \text{ \AA}$ (2.4 pixels) for the JH -band. Thus, the systematic error in redshifts are 0.0006 in the K -band and 0.0015 in the JH -band.

3. Results

The final JHK spectra are shown in figure 1. The JH -band spectrum was calibrated from the H -band photometry and the K -band spectrum from the K' -band pho-

tometry of Yamada et al. (in preparation). A $1''.0 \times 2''.1$ aperture, aligned with the position angle used for the spectroscopy, was used in both cases.

3.1. Emission Lines

We detected emission lines of [O II] $\lambda 3727$, H β , [O III] $\lambda\lambda 4959, 5007$, H α + [N II] $\lambda\lambda 6548, 6583$ and [S II] $\lambda\lambda 6716, 6731$. [Ne III] $\lambda 3869$ may be present, but this region is contaminated with the edge of the Balmer discontinuity. None of the emission lines was resolved at the wavelength resolutions of OHS/CISCO, which were 700 km s^{-1} in the K -band, and 1500 km s^{-1} in the JH -band.

Due to the low wavelength resolution, the H α and [N II] lines were blended, as was the [S II] doublet. We deconvolved these lines by fitting multiple Gaussian profiles. For H α + [N II], we assumed [N II] $\lambda 6583$ /[N II] $\lambda 6548 = 3.0$ and demanded that all three lines have the same width. For the [S II] doublet, we fixed the line widths to be equal to results from the H α + [N II] fitting. The results are given in figure 2. The derived line ratios were [N II] $\lambda 6583$ /H $\alpha = 2.3 \pm 0.6$ and [S II] $\lambda 6716$ /[S II] $\lambda 6731 = 0.61 \pm 0.44$ (2σ). Other lines were fitted by single Gaussian profiles to obtain their redshifts and to determine the continuum level; we assumed a common redshift and line widths for [O II], H β , and [O III]. The emission-line properties are listed in table 1. The fluxes of [O II], H β , and [O I] are the value above the continuum level. The fluxes of the other lines are determined from the results of Gaussian fitting, because they are blended. The redshift difference between lines in the JH - and K -bands might arise from a systematic error in the wavelength calibration.

The contribution to the broad-band fluxes from the emission lines is very large, amounting to 22% in the J -band, 30% in the H and 42% in the K' -band.

We show the spatial intensity profiles of the continuum and emission lines along the slit in figure 3. The profiles of both [O III] and H α + [N II] are clearly more extended than the adjacent continua. We estimate of the spatial extent of the line emission to be roughly $0''.7$ – $0''.8$, or 6–7 kpc.

3.2. Detection of Balmer Discontinuity

The high sensitivity of OHS allows the continuum of 53W002 to be clearly detected. We show the SED of the continuum in figure 4 with a solid line. We removed all of the emission-lines, except for [Ne III], using the results of the Gaussian profile fitting, and then smoothed the resulting spectrum with a $0.05 \mu\text{m}$ boxcar filter.

A clear break in the continuum is seen at $1.3 \mu\text{m}$, which is the first spectroscopic detection of the Balmer discontinuity in a high-redshift radio galaxy. The [Ne III] emission line, which we disregarded above, is located here, and may have affected the position of this break.

To check the effect of this emission line, we subtract a Gaussian at the position of the line, assuming [Ne III] $\lambda 3869$ /[O II] $\lambda 3727 = 0.2$ which was the result of simulations from CLOUDY94 carried out in the following analysis. The continuum thus derived is displayed with a dotted line in figure 4, and shows a slight shift in the position of the break.

4. Discussion

4.1. Nature of Emission-Line Clouds

We measure H α /H $\beta = 3.4$. If we adopt an intrinsic value of 3.1 (Osterbrock 1989) and the SMC extinction curve of Pei (1992) with $A_V/E(B-V) = 3.1$, we derive $E(B-V) = 0.14$. The extinction-corrected emission line fluxes are listed in the fifth column of table 1.

The sulfur line ratio is a good indicator of the electron density (Osterbrock 1989), and our measured value of [S II] $\lambda 6716$ /[S II] $\lambda 6731 = 0.61 \pm 0.44$ implies $n_e \sim 1 \times 10^3 \text{ cm}^{-3}$. The 2σ lower limit is $n_e \sim 5 \times 10^2 \text{ cm}^{-3}$, but we cannot constrain the upper limit.

The L α flux is $2.8 \times 10^{-19} \text{ W m}^{-2}$ (Keel et al. 1999). Because the L α morphology is smaller than our slit size of $1''.0$ (Windhorst et al. 1998), we estimate the $L(\text{L}\alpha)/L(\text{H}\beta)$ ratio to be 3.2. The correction for the Galactic extinction of $E(B-V) = 0.03$ (Burstein, Heiles 1982) produces $L(\text{L}\alpha)/L(\text{H}\beta) = 3.5$. A further correction for the *in situ* extinction of $E(B-V) = 0.14$ results in $L\alpha/\text{H}\beta = 17$, which is consistent, given the uncertainty in the extinction, with a low-density value of 23 (Ferland, Osterbrock 1985).

In figure 5 we present two emission-line ratio diagrams. One shows [N II] $\lambda 6583$ /H α versus [O III] $\lambda 5007$ /H β and the other [O II] $\lambda 3727$ /[O III] $\lambda 5007$ versus [O III] $\lambda 5007$ /H β . We plot the location of 53W002 together with the ratios of narrow-line AGNs; H II regions taken from the literature. The radio galaxy lies in the region occupied by narrow line AGNs and the emission-line cloud is therefore ionized by a hidden nucleus.

To investigate the physical state of the emission-line cloud, we carried out photoionization calculations using the code CLOUDY94 (Ferland 1999, 2000). We assume a spectral index of $\alpha = -0.7$ for the ionizing continuum, taken from the composite spectra of radio-loud QSOs (Cristiani, Vio 1990; Zheng et al. 1997). The observed line ratios are reproduced with $Z \sim Z_\odot$, $\log U \sim -3$, and $n_e = 1 \times 10^{3-4} \text{ cm}^{-3}$ (see solid and dashed lines in figure 5). We could not reproduce the observed ratios with an $\alpha = -1.5$ power law continuum (dot-dashed lines in figure 5), nor by models with $0.1 Z_\odot$ metallicity (dashed-long-dashed lines in figure 5).

We then estimated the mass of ionized gas from the physical values derived above and the H α line luminosity,

using the following equations:

$$L_{\text{H}\alpha} = n_e^2 \alpha_{\text{H}\alpha}^{\text{eff}} h \nu_{\text{H}\alpha} V f, \quad (1)$$

$$M_{\text{gas}} = V f n_e m_{\text{H}}, \quad (2)$$

where h is the Planck constant, $\nu_{\text{H}\alpha}$ the frequency of the $\text{H}\alpha$ line, V the volume of the line-emitting cloud, f the filling factor, m_{H} the hydrogen mass, and $\alpha_{\text{H}\alpha}^{\text{eff}} = 6.04 \times 10^{-14} (\text{cm}^3 \text{s}^{-1})$ (Osterbrock 1989) the $\text{H}\alpha$ recombination coefficient under Case B. We derive a gas mass of $10^{7-8} M_{\odot}$.

A rough estimate of the filling factor, f , of the cloud can be made by assuming the cloud to be a sphere of 3 kpc radius (section 3.1). We calculate $f \sim 10^{-5}-10^{-7}$, consistent with the typical values of low- z radio galaxies of $10^{-4}-10^{-6}$ (Heckman et al. 1982; van Breugel et al. 1985).

High-resolution HST imaging shows the presence of an extended blue cloud which peaks $0'.45$ west of the nucleus (Windhorst et al. 1998). Our emission-line region, however, almost coincides with the continuum core. Therefore, what we are seeing is not those blue clouds, but a cloud which envelops the whole galaxy. This gas could be a remnant of a previous merger event, resulting in the starburst activity observed in our spectra as the Balmer discontinuity (see section 4.2.2). Metallicity as high as Z_{\odot} might be produced during this period.

4.2. SED and Age of the Host Galaxy

The spectral energy distribution of 53W002 is shown by the open circles and squares in figure 6. The optical data were taken from Windhorst et al. (1991) and the infrared data from line-free regions of our spectra. An additional data point was derived from the continuum after subtracting the $[\text{Ne III}]$ line assuming $[\text{Ne III}]/[\text{O II}] = 0.2 \pm 0.1$. Because Windhorst et al. (1991) measured the total magnitudes, our infrared data were multiplied by a factor of 1.2 to match their H - and K -band photometry. We disregard the U -band data of Windhorst et al. (1991), which is shortward of $L\alpha$ in the rest-frame, and is likely to be strongly attenuated by the $L\alpha$ forest from the surrounding objects.

Next, we removed two non-stellar components from the SED. One is the nebular continuum emission and the other is the scattered light from the hidden nucleus.

The strength of the nebular continuum was calculated from the $\text{H}\beta$ emission line flux using the tabulated coefficients of Aller (1984) for $T_e = 1 \times 10^4 \text{ K}$. We ignore the contribution from He recombination, which our CLOUDY94 simulations indicate will be weak.

We assume the intrinsic shape of the continuum from the hidden nucleus to be an $\alpha = -0.7$ power law. Since we do not know whether the scatterers are dust grains or electrons, we consider both cases. Because electron-scattering is achromatic, the scattered spectrum is the

same as the incident spectrum, while the dust-scattered spectrum was from Cimatti et al. (1994). After applying the extinction of $E(B - V) = 0.14$, the flux was scaled to match the upper limits of the scattered AGN contribution estimated by Windhorst et al. (1998) as shown in figure 6.

The resulting SEDs of the underlying stellar population, after subtracting these two components, is shown by the filled circles and triangles in figure 6. We tried to fit these SEDs with a few models of galactic spectra.

4.2.1. One-component model

First, we fitted these SEDs with single-component synthetic spectra produced by the spectrophotometric galaxy evolution code PEGASE (Fioc, Rocca-Volmerange 1997), to which an extinction of $E(B - V) = 0.14$ was applied. Instead of the SMC extinction curve, we applied the extinction curve of Calzetti et al. (1994), which is an empirical relation for the stellar UV continuum derived from the spectra of nearby starburst regions. We considered three star-formation histories — an instantaneous burst, and two exponential bursts with e -folding times of 200 Myr and 1 Gyr — and the age was left as a free parameter. We adopted the Scalo IMF. We also fit our models to the observed SED, to investigate the effect of subtracting the non-stellar emission. These results are given in table 2.

The results are not very sensitive to the assumed non-stellar contributions, since the age of the galaxy is mainly determined by the strength of the Balmer discontinuity. Although the fitted parameters vary according to the assumed star-formation history, the age is always young: 70–700 Myr, corresponding to a formation redshift $z_{\text{form}} = 2.5-3.2$.

Windhorst et al. (1991) showed, from the far-UV SED and possible detections of UV absorption lines, that the main-sequence cutoff age is 250–320 Myr, so we adopt the $\tau = 200$ Myr model in the following discussions. The stellar mass of the galaxy is then $\sim 10^{11} M_{\odot}$, which is of the order of that of an L^* galaxy.

4.2.2. Two-component model

According to the high-resolution HST imaging, 53W002 has a radial color gradient, suggesting that the outskirts of the galaxy is comprised of older stars (0.5–1 Gyr; Windhorst et al. 1994). There may therefore have been additional star-formation episodes prior to the current one, and we attempt to fit the SED with two stellar components to evaluate how much stellar mass was created by the current starburst activity.

The models consisted of an old component of fixed age and a younger component of unknown age. A $\tau = 200$ Myr exponential burst with Scalo IMF was assumed for both components. We varied the fraction of the initial

gas mass in the old component from 0.1 to 0.9 in 0.1 steps. Two ages for the old component were assumed: one is 1 Gyr, the age suggested by Windhorst et al. (1994); the other is 3 Gyr, the maximum age allowed by the age of the universe. The results of the model fitting are shown in table 3 and figure 7.

The χ^2 -test was used to assess the results of the fitting. We reject models which are not consistent with the data at the 99% confidence level, which corresponds to $\chi^2 > 25$. We therefore exclude models where the mass fraction of old component is 0.9 or larger. We also reject models which produce an age of less than 200 Myr for the current burst, which is a lower limit derived from the UV spectrum (Windhorst et al. 1991), and only those models whose old mass fraction is less than 0.7 remain. We therefore conclude that 53W002 is undergoing a massive starburst, and that at least 1/3 of its stellar mass is forming in the current burst.

4.2.3. Mass and formation of 53W002

We next compare the stellar mass with those of other radio galaxies in the literatures. Because these mass estimations were carried out by single-component SED fitting, we use the mass of 53W002 derived using the one-component model.

The stellar mass of the galaxy was estimated to be less than $1.4 \times 10^{11} M_{\odot}$ by the one-component model, similar to that of $z = 1.824$ radio galaxy 3C 256 (Simpson et al. 1999). This galaxy also underwent a recent starburst and its stellar mass is only $1.2 \times 10^{11} M_{\odot}$ (converted to our adopted cosmology). Best et al. (1998) estimated the masses of 26 $z \sim 1$ 3C radio galaxies using the GISSEL spectral synthesis codes of Bruzual and Charlot (1993), and derived a median value of $4.4 \pm 1.7 \times 10^{11} M_{\odot}$ (again, converted to our adopted cosmology). We determine that the effect of the different IMFs used is only 10%, and therefore conclude that the mass of 53W002 is less than 1/3 of a typical $z \sim 1$ 3C radio galaxy. However, Eales et al. (1997) reported a correlation between the radio and *K*-band luminosities of $z \sim 1$ radio galaxies, and the radio luminosity of 53W002 is similar to those of the B2/6C radio galaxies, which are on average ~ 0.6 mag fainter than the 3C objects. If we assume that the stellar mass correlates with the *K*-band luminosity, the mass of $z \sim 1$ B2/6C radio galaxies is $\sim 2.5 \times 10^{11} M_{\odot}$, which is still twice the value of 53W002.

There are 17 candidate $L\alpha$ -emitters in the field of 53W002, and 7 of them have been spectroscopically confirmed to lie at the same redshift as the radio galaxy (Pascarelle et al. 1996a,b,1998; Keel et al. 1999). These objects are of sub-galactic size, and were postulated to be ‘building blocks’ which will merge into a luminous galaxy by the present epoch. If 53W002 experiences additional starburst activity every 500 Myr by merging with these

surrounding sub-galactic clumps, it will grow into a massive galaxy of a few $\times 10^{11} M_{\odot}$ by $z = 1$. These results strongly support the hypothesis that 53W002 is a forming massive elliptical galaxy undergoing multiple merger events, and an ancestor of present-day luminous galaxies.

5. Summary

We have performed infrared *JHK* spectroscopy of the weak radio galaxy 53W002 at $z = 2.39$, using CISCO and the newly commissioned instrument OHS on the Subaru telescope.

We detected the rest-frame optical emission lines of [O II] $\lambda 3727$, H β , [O III] $\lambda \lambda 4959, 5007$, H α , [N II] $\lambda \lambda 6548, 6583$ and [S II] $\lambda \lambda 6716, 6731$. These emission lines were reproduced by a model cloud with $Z \sim Z_{\odot}$, $\log U \sim -3$, and $n_e = 1 \times 10^{3-4} (\text{cm}^{-3})$, ionized by an $\alpha = -0.7$ power-law continuum. The mass of ionized gas in the cloud was estimated to be $M_{\text{gas}} = 10^{7-8} M_{\odot}$, and the filling factor was calculated to be as small as $10^{-5-10^{-7}}$, indicating significant clumpiness. We found no offset between the peak positions of the line and continuum emission, which suggests that the emission line cloud is not the extended blue cloud reported in Windhorst et al. (1998).

The Balmer discontinuity was detected clearly for the first time in the continuum of a high-redshift radio galaxy. We were able to fit the rest-frame UV–optical continuum by a 70–700 Myr-old stellar population. A fit with two-component model indicated that at least one-third of the total stellar mass is involved in the current starburst. We estimated the total stellar mass to be $1-1.4 \times 10^{11} M_{\odot}$ by one-component model, which is smaller than typical $z \sim 1$ B2/6C radio galaxies. The mass becomes twice as much if we introduce the two-component model, but is still smaller than that of $z \sim 1$ 3C radio galaxies. We therefore conclude that 53W002 is now assembling a large part of its stellar mass through mergers with the surrounding sub-galactic objects, and will end up as a massive elliptical observed today.

We are indebted to all staff members of the Subaru telescope, NAOJ. We appreciate M. Fioc and B. Rocca-Volmerange for generously offering their galaxy modeling code, PEGASE and G. Ferland for the spectral synthesis code CLOUDY94.

References

- Aller, L. H. 1984, *Physics of Thermal Gaseous Nebulae* (Dordrecht: Reidel), p.98
- Alloin, D., Barvainis, R., & Guilleaume, S. 2000, *ApJ*, 528, L81
- Best, P. N., Longair, M. S., & Röttgering, H. J. A. 1998, *MNRAS*, 295, 549

- Burstein, D., & Heiles, C. 1982, *AJ*, 87, 1165
- Buzual, G., & Charlot, S. 1993, *ApJ*, 405, 538
- Calzetti, D., Kinney, A. L., & Storchi-Bergmann, T. 1994, *ApJ*, 429, 582
- Cimatti, A., di Serego Alighieri, S., Field, G. B., & Fosbury, R. A. E. 1994, *ApJ*, 422, 562
- Costero, R., & Osterbrock, D. E. 1977, *ApJ*, 211, 675
- Cristiani, S., & Vio, R. 1990, *A&A*, 227, 385
- Eales, S. A., & Rawlings, S. 1993, *ApJ*, 411, 67
- Eales, S. A., Rawlings, S., Law-Green, D., Cotter, G., & Lacy, M. 1997, *MNRAS*, 291, 593
- Fioc, M., & Rocca-Volmerange, B. 1997, *A&A*, 326, 950
- Ferland, G. J. 2000, *Rev. Mex. Astron. Astrofis.*, 9, 153
- Ferland, G. J. 1999, in *ASP Conf. Ser.* 216, *Astronomical Data Analysis Software and Systems IX*, ed. N. Manset, C. Veillet, & D. Crabtree (San Francisco: ASP), 32
- Ferland, G. J., & Osterbrock, D. E. 1985, *ApJ*, 289, 105
- French, H. B. 1980, *ApJ*, 240, 41
- Heckman, T. M., Miley, G. K., Balick, B., van Breugel, W. J. M., & Butcher, H. R. 1982, *ApJ*, 262, 529
- Iwamuro, F., Motohara, K., Maihara, T., Hata, R., & Harashima, T. 2001, *PASJ*, 53, 355
- Keel, W. C., Cohen, S. H., Windhorst, R. A., & Waddington, I. 1999, *AJ*, 118, 2547
- Koski, A. T. 1978, *ApJ*, 223, 56
- Maihara, T., Iwamuro, F., Oya, S., Tsukamoto, H., Hall, D. N., Cowie, L. L., Tokunaga, A. T., & Pickles, A. J. 1994, *Proc. SPIE*, 2198, 194
- McCall, M. L., Rybski, P. M., & Shields, G. A. 1985, *ApJS*, 57, 1
- Motohara, K., Maihara, T., Iwamuro, F., Oya, S., Imanishi, M., Terada, H., Goto, M., Iwai, J., et al. 1998, *Proc. SPIE*, 3354, 659
- Osterbrock, D. E. 1989, *Astrophysics of Gaseous Nebulae and Active Galactic Nuclei* (Mill Valley: University Science Books)
- Pascarelle, S. M., Windhorst, R. A., Driver, S. P., Ostrand, E. J., & Keel, W. C. 1996a, *ApJ*, 456, L21
- Pascarelle, S. M., Windhorst, R. A., Keel, W. C., & Odewahn, S. C. 1996b, *Nature*, 383, 45
- Pascarelle, S. M., Windhorst, R. A., & Keel, W. C. 1998, *AJ*, 116, 2659
- Pei, Y. C. 1992, *ApJ*, 395, 130
- Pettini, M., Kellogg, M., Steidel, C. C., Dickinson, M., Adelberger, K. L., & Giavalisco, M. 1998, *ApJ*, 508, 539
- Simpson, C., Eisenhardt, P., Armus, L., Chokshi, A., Dickinson, M., Djorgovski, S. G., Elston, R., Jannuzi, B. T., et al. 1999, *ApJ*, 525, 659
- Scoville, N. Z., Yun, M. S., Windhorst, R. A., Keel, W. C., & Armus, L. 1997, *ApJ*, 485, L21
- van Breugel, W. J. M., Miley, G., Heckman, T., Butcher, H., & Bridle, A. 1985, *ApJ*, 290, 496
- Veilleux, S., & Osterbrock, D. E. 1987, *ApJS*, 63, 295
- Windhorst, R. A., Burstein, D., Mathis, D. F., Neuschaefer, L. W., Bertola, F., Buson, L. M., Koo, D. C., Matthews, K., Barthel, P. D., & Chambers, K. C. 1991, *ApJ*, 380, 362
- Windhorst, R. A., Gordon, J. M., Pascarelle, S. M., Schmidtke, P. C., Keel, W. C., Burkey, J. M., & Dunlop, J. S. 1994, *ApJ*, 435, 577
- Windhorst, R. A., Keel, W. C., & Pascarelle, S. M. 1998, *ApJ*, 494, L27
- Yamada, T., Ohta, K., Tomita, A., & Takata, T. 1995, *AJ*, 110, 1564
- Zheng, W., Kriss, G. A., Telfer, R. C., Grimes, J. P., & Davidson, A. F. 1997, *ApJ*, 475, 469

Fig. 1. *JHK* spectra of 53W002. The lower trace shows the 1σ noise level calculated from the background level. Many strong forbidden lines and weak $H\beta$ line are present. Due to the low-wavelength resolution, $H\alpha + [N\text{ II}] \lambda\lambda 6548, 6583$ and $[S\text{ II}] \lambda\lambda 6716, 6731$ are blended.

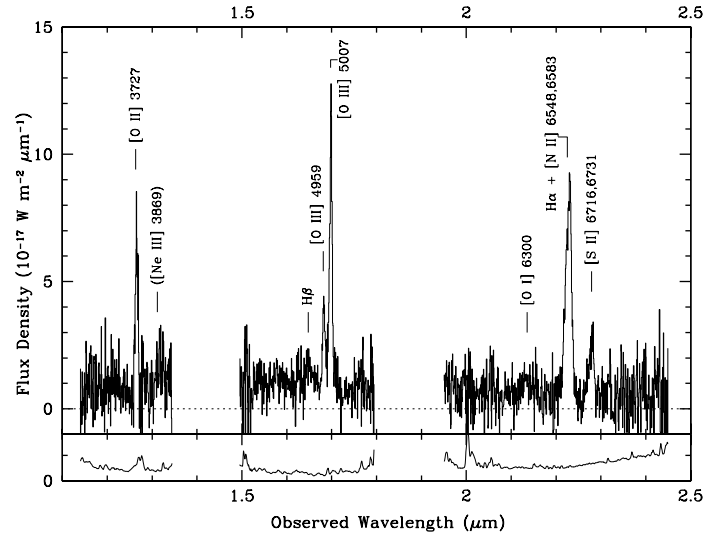


Fig. 2. Deconvolution of the blended $H\alpha + [N\text{ II}]$ and $[S\text{ II}]$ lines.

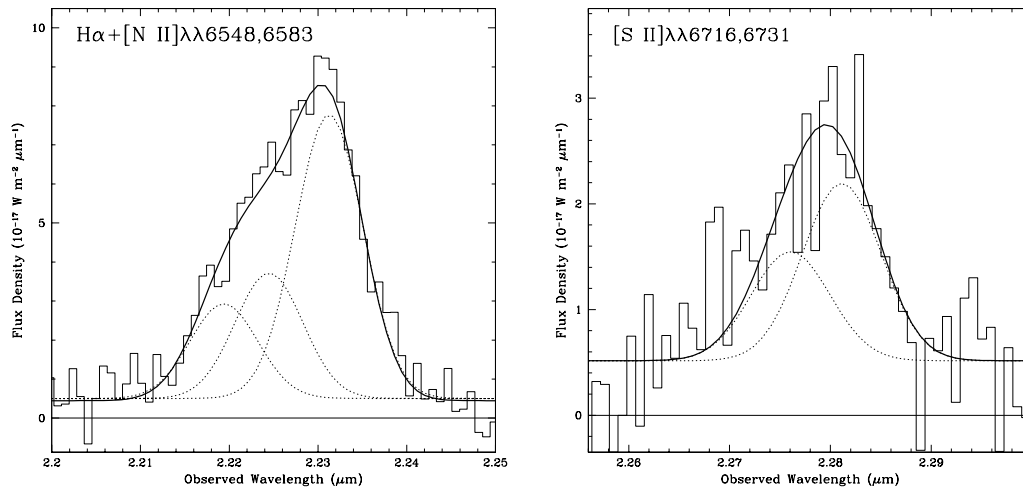


Fig. 3. Spatial profiles of the spectra of 53W002. In the upper panels, west is to the right, while south-east is to the right in the lower two. The dotted lines are fitted Gaussian profiles. Both $[\text{O III}]$ and $\text{H}\alpha + [\text{N II}]$ lines are more spatially extended than the continuum. The seeing sizes for the H -band and K -band spectra are $0''.6$ and $0''.4$, respectively.

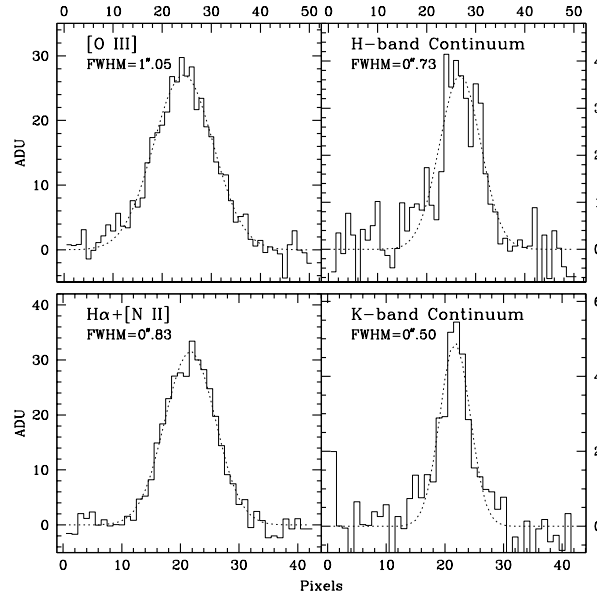


Fig. 4. Continuum of 53W002. All of the emission lines, except $[\text{Ne III}]$, have been subtracted by Gaussian fitting, and the resulting spectrum has been smoothed with a $0.05 \mu\text{m}$ boxcar filter. The solid line shows the raw continuum, while the dotted line shows further subtraction of $[\text{Ne III}]$, where we have assumed $[\text{Ne III}]/[\text{O II}] = 0.2$ (see text).

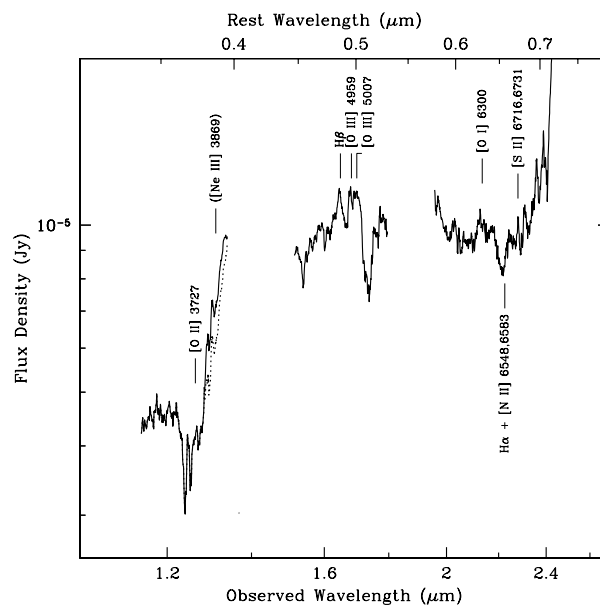


Fig. 5. Reddening corrected line ratios of 53W002 (open circle with error bars) plotted together with those of Seyfert 2s (filled circles), radio galaxies (filled squares), H II regions (open circles), H II galaxies (open circles), and starburst galaxies (open triangles) taken from the literature (Veilleux, Osterbrock 1987; McCall et al. 1985; French 1980; Koski 1978; Costero, Osterbrock 1977). The results of photoionization calculations carried out using CLOUDY94 are indicated by the lines. Solar metallicity and a spectral index of $\alpha = -0.7$ for the ionizing continuum were assumed, except for one case where we assumed $\alpha = -1.5$ (thin dot-dashed line), and one case of $Z = 0.1Z_{\odot}$ (thin dash-long-dashed line). The ionization parameter (U) varies along each line, with representative points labeled by the value of $\log U$.

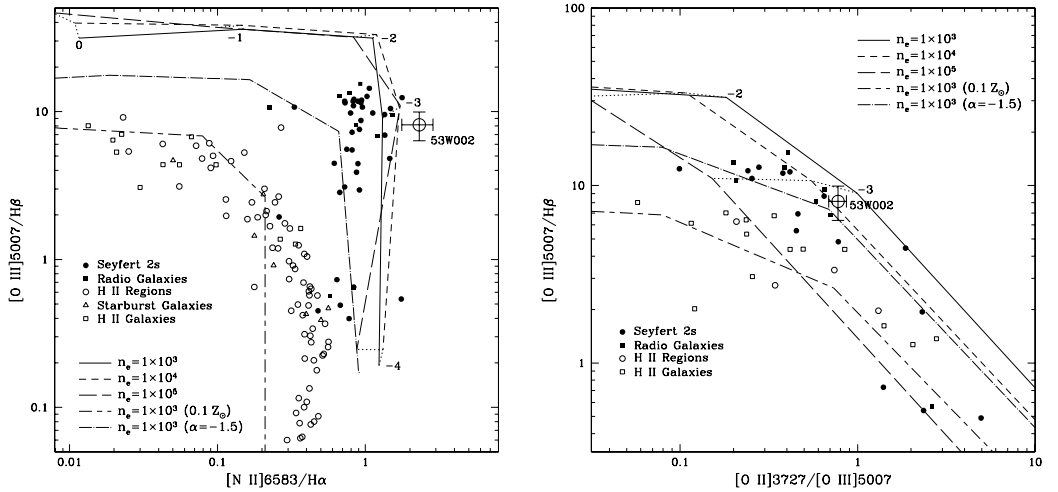


Fig. 6. Spectral energy distributions of 53W002. Open circles and triangles are observed values from the present observations and Windhorst et al. (1991), respectively. The assumed AGN and nebular continuum components were subtracted (see text) to produce the SED of the stellar component alone, which is shown by the filled symbols. The filled squares indicate the upper limit of the unresolved AGN component determined from HST observations (Windhorst et al. 1998). The nebular continuum was calculated from the $H\beta$ flux, and is shown by the long dashed line. The solid lines show the best-fit one-component spectral model. The dashed line shows the AGN contribution, which is assumed to be dust-scattered in the left panel, and electron-scattered in the right panel.

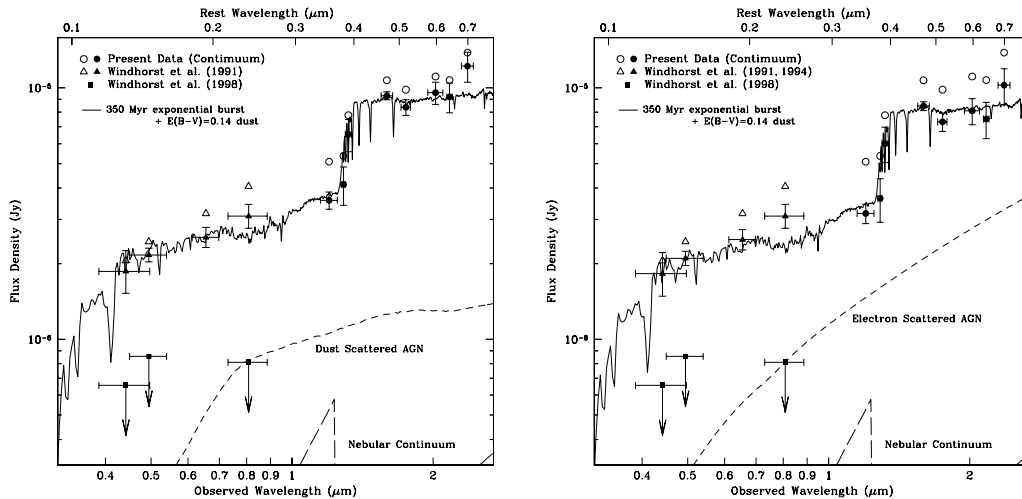


Fig. 7. Results of fitting two-component models to the stellar SED of 53W002. The AGN component is assumed to be a dust-scattered power-law. The dotted lines show the spectra of the old component, while the dashed lines show that of the current burst.

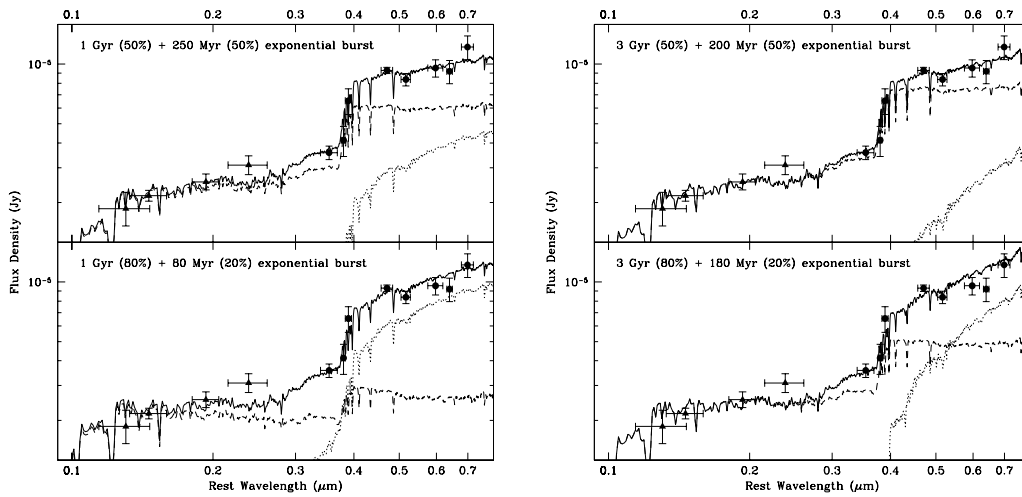


Table 1. Emission line properties of 53W002. All errors are 2σ .

Line	λ_{rest} (\AA)	Redshift*	Flux ($\times 10^{-19} \text{ W m}^{-2}$)	Flux (corrected) ($\times 10^{-19} \text{ W m}^{-2}$)	Continuum ($\times 10^{-18} \text{ W m}^{-2} \mu\text{m}$)	EW_{rest} (\AA)
[O II]	3727	2.3923 \pm 0.0004	4.8 \pm 0.4	8.8 \pm 0.8	6.2 \pm 1.3	230 \pm 50
H β	4861	2.3923 \pm 0.0004	0.88 \pm 0.18	1.4 \pm 0.3	10.3 \pm 0.8	20 \pm 8
[O III]	4959	2.3923 \pm 0.0004	2.1 \pm 0.3	3.3 \pm 0.4	10.3 \pm 0.9	61 \pm 9
[O III]	5007	2.3923 \pm 0.0004	7.3 \pm 0.5	11.3 \pm 0.8	10.3 \pm 0.9	210 \pm 20
[O I]	6300	2.3833 \pm 0.0076	0.76 \pm 0.36	1.1 \pm 0.5	5.9 \pm 1.4	37 \pm 20
H α	6563	2.3895 \pm 0.0008	3.1 \pm 0.7	4.3 \pm 0.9	5.0 \pm 1.6	180 \pm 70
[N II]	6583	2.3895 \pm 0.0008	7.2 \pm 0.8	9.9 \pm 1.1	5.0 \pm 1.6	420 \pm 140
[S II]	6716	2.3890 \pm 0.0032	1.0 \pm 0.7	1.4 \pm 1.0	5.2 \pm 2.5	60 \pm 60
[S II]	6731	2.3890 \pm 0.0032	1.6 \pm 0.7	2.2 \pm 1.0	5.2 \pm 2.5	90 \pm 70

* No systematic errors are included.

Table 2. Parameters for the best-fit models of the spectral energy distribution.

Galaxy evolution model	Non-stellar*	χ^2	Age (Myr)	Stellar mass (M_{\odot})	SFR ($M_{\odot} \text{ yr}^{-1}$)
Instantaneous burst	N	19.1	80	9.7×10^{10}	0
	E	19.0	70	6.8×10^{10}	0
	D	19.1	80	8.1×10^{10}	0
Exponential burst ($\tau = 200$ Myr)	N	21.3	350	1.3×10^{11}	1.5×10^2
	E	12.5	350	9.7×10^{10}	1.1×10^2
	D	10.0	350	1.1×10^{11}	1.2×10^2
Exponential burst ($\tau = 1$ Gyr)	N	23.8	600	1.4×10^{11}	1.8×10^2
	E	11.0	600	1.1×10^{11}	1.4×10^2
	D	8.9	700	1.3×10^{11}	1.4×10^2

* Model of non-stellar components. N: No non-stellar component is assumed. D: Nebular continuum + dust scattered $\alpha = -0.7$ power law. E: Nebular continuum + electron scattered $\alpha = -0.7$ power law.

Table 3. Best-fit two-components models of the spectral energy distribution.

Age of old component		1 Gyr				3 Gyr	
Non-stellar*	Old frac.†	χ^2	Age‡ (Myr)	Stellar mass (M_\odot)	χ^2	Age‡ (Myr)	Stellar mass (M_\odot)
D	0.1	9.5	350	1.5×10^{11}	9.2	350	1.2×10^{11}
	0.2	11.4	350	1.6×10^{11}	9.0	350	1.3×10^{11}
	0.3	8.9	300	1.6×10^{11}	9.9	350	1.5×10^{11}
	0.4	10.0	300	1.7×10^{11}	9.6	300	1.5×10^{11}
	0.5	8.6	250	1.8×10^{11}	8.4	300	1.7×10^{11}
	0.6	9.5	200	1.9×10^{11}	11.8	300	2.1×10^{11}
	0.7	9.8	160	2.1×10^{11}	12.2	250	2.3×10^{11}
	0.8	13.3	80	2.4×10^{11}	18.7	180	2.7×10^{11}
	0.9	84.4	40	2.9×10^{11}	45.8	70	3.7×10^{11}
E.....	0.1	12.4	300	1.3×10^{11}	13.5	300	9.3×10^{10}
	0.2	11.2	300	1.4×10^{11}	12.1	300	1.0×10^{11}
	0.3	12.8	300	1.5×10^{11}	11.3	300	1.2×10^{11}
	0.4	11.7	250	1.5×10^{11}	11.7	300	1.4×10^{11}
	0.5	14.2	250	1.6×10^{11}	14.6	300	1.6×10^{11}
	0.6	13.1	180	1.7×10^{11}	13.8	250	1.7×10^{11}
	0.7	14.6	140	1.9×10^{11}	18.1	200	1.9×10^{11}
	0.8	19.5	50	2.2×10^{11}	24.4	160	2.4×10^{11}
	0.9	103.4	40	2.6×10^{11}	54.5	60	3.4×10^{11}

* Model of non-stellar components. D: Nebular continuum + dust scattered $\alpha = -0.7$ power law. E: Nebular continuum + electron scattered $\alpha = -0.7$ power law.

† Mass fraction of old component.

‡ Age of current burst component.